

CHANDRA OBSERVATIONS OF THE COLLISIONAL RING GALAXY NGC 922

A. H. PRESTWICH¹, J. L. GALACHE¹, T. LINDEN², V. KALOGERA³, A. ZEAS^{1,4,5}, T. P. ROBERTS⁶,
R. KILGARD⁷, A. WOLTER⁸, AND G. TRINCHIERI⁸

¹ Harvard-Smithsonian Center for Astrophysics, 60 Garden Street, Cambridge, MA 02138, USA

² University of Santa Cruz, Department of Physics 211 Interdisciplinary Sciences Building, 1156 High Street, Santa Cruz, CA 95064, USA

³ Center for Interdisciplinary Exploration and Research in Astrophysics (CIERA) & Department of Physics and Astronomy,
Northwestern University, 2145 Sheridan Road, Evanston, IL 60208, USA

⁴ University of Crete, Physics Department, 71003 Heraklion, Crete, Greece

⁵ Foundation for Research and Technology-Hellas, 71110 Heraklion, Crete, Greece

⁶ Department of Physics, University of Durham, South Road, Durham DH1 3LE, UK

⁷ Van Vleck Observatory, Wesleyan University, 96 Foss Hill Dr., Middletown, CT 06459, USA

⁸ INAF, Osservatorio Astronomico di Brera, Via Brera 28, IT 20121 Milano, Italy

Received 2011 June 15; accepted 2012 January 3; published 2012 February 24

ABSTRACT

In this paper, we report on *Chandra* observations of the starburst galaxy NGC 922. NGC 922 is a drop-through ring galaxy with an expanding ring of star formation, similar in many respects to the Cartwheel galaxy. The Cartwheel galaxy is famous for hosting 12 ultraluminous X-ray sources (ULXs), most of which are in the star-forming ring. This is the largest number of ULXs seen in a single system and has led to speculation that the low metallicity of the Cartwheel ($0.3 Z_{\odot}$) may optimize the conditions for ULX formation. In contrast, NGC 922 has metallicity near solar. The *Chandra* observations reveal a population of bright X-ray sources, including seven ULXs. The number of ULXs in NGC 922 and the Cartwheel scales with the star formation rate: we do not find any evidence for an excess of sources in the Cartwheel. Simulations of the binary population in these galaxies suggest that the ULX population in both systems is dominated by systems with strong wind accretion from supergiant donors onto direct-collapse black holes. The simulations correctly predict the ratio of the number of sources in NGC 922 and the Cartwheel. Thus, it would appear that the metallicity of the Cartwheel is not low enough to see a difference in the ULX population compared to NGC 922.

Key words: galaxies: individual (NGC 922) – X-rays: galaxies

Online-only material: color figures

1. INTRODUCTION

Chandra images of starburst galaxies are spectacular, showing a multitude of bright point sources and plumes of X-ray emitting gas (Fabbiano 2006). The brightest of the discrete sources ($L_x > 10^{39}$ erg s⁻¹) are known as ultraluminous X-ray sources (ULXs), and have attracted considerable attention in recent years because they have broadband X-ray luminosities many times the Eddington limit for a neutron star or stellar mass black hole (e.g., Zezas et al. 2002). There is a growing consensus that most ULXs can be explained as high ($\geq 10 M_{\odot}$) stellar mass black holes radiating in excess of the Eddington limit, possibly with mild beaming (see Roberts 2007, and references therein). The most massive stellar black holes are thought to form in low-metallicity environments, where the stellar winds of the progenitor are relatively weak and do not carry off such a large fraction of the initial mass of the star (Belczynski et al. 2004). Thus, ULXs should form preferentially in low-metallicity environments. Observational evidence for this is seen in some ULXs (e.g., Soria et al. 2005)

NGC 922 is a peculiar galaxy with a distinctive C-shaped ring of H α emission (see Figure 1). It has been described as a dust-obscured grand design spiral galaxy (Block et al. 2001). However, a recent paper by Wong et al. (2006) presents compelling evidence that the morphology could be explained as a result of an off-center collision between a spiral and its dwarf companion. This model successfully explains the C-shaped morphology. The intruder galaxy is identified to be a dwarf galaxy approximately 8 arcmin away, apparently connected to NGC 922 by a plume of tidal debris. The starburst in NGC 922

is still on-going as evidenced by the luminous H α emission and a population of very young, massive star clusters (Pellerin et al. 2010). NGC 922 is similar to the Cartwheel in that both of them are the remnants of drop through collisions, and both of them have high star formation rates. The Cartwheel galaxy is famous for hosting 12 ULXs, most of which are in the star-forming ring (Wolter & Trinchieri 2004, see also Gao et al. 2003). This is the largest number of ULXs seen in a single system and has led to speculation that the low metallicity of the Cartwheel ($0.3 Z_{\odot}$) may optimize the conditions for ULX formation (Mapelli et al. 2009). In contrast, NGC 922 has metallicity near solar (Wong et al. 2006). We are currently engaged in a *Chandra* and *Hubble Space Telescope* (*HST*) study of the X-ray binary population of NGC 922. In this paper, we compare the ULX population of NGC 922 and the Cartwheel. Our primary goal is to determine whether there is an excess of ULXs (normalized to the star formation rate) in the Cartwheel compared to NGC 922 that can be attributed to the difference in metallicity. In addition, we use population synthesis models to estimate the expected number of ULXs in both systems. In a future paper, we use *HST* broad band and H α images to study the relationship between the X-ray sources and star clusters in NGC 922.

2. DATA ANALYSIS

Two images of NGC 922 were obtained in 2009. The first was a 30 ks exposure designed to detect X-ray point sources down to a luminosity of 7×10^{38} erg s⁻¹ and the second a 10 ks exposure, scheduled a few months later, to detect variability in the brightest

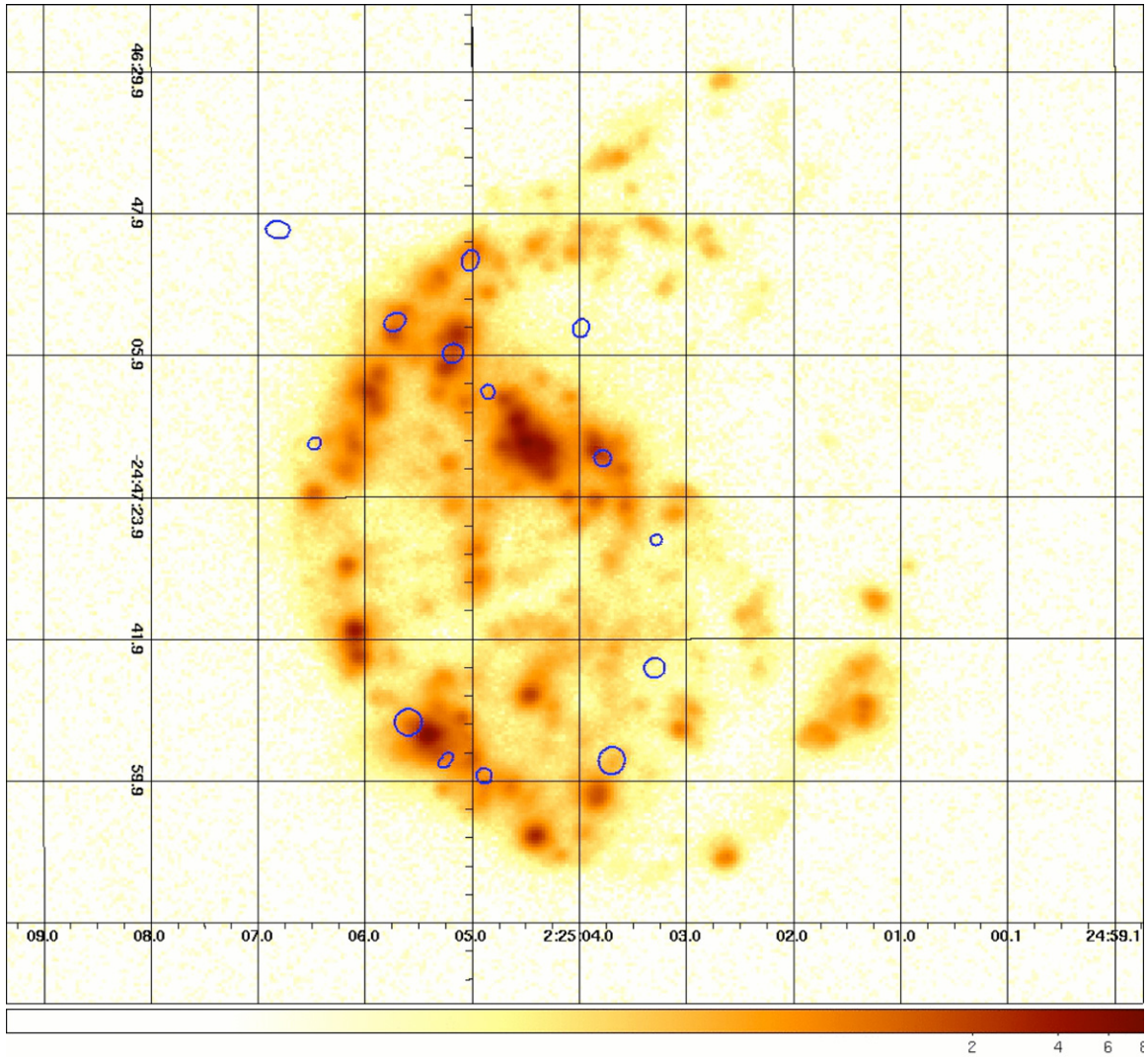


Figure 1. $H\alpha$ image of NGC 922 with positions of X-ray sources marked. The $H\alpha$ image is from Meurer et al. (2006), downloaded via the NASA Extragalactic Database.

(A color version of this figure is available in the online journal.)

Table 1
Observing Configuration for Two *Chandra* Observations of NGC 922

ObsID	Date	Exposure Time (ks)	Chip	Data Mode	Exposure Mode
10563	2009 Mar 5	29.737	S3	TIMED EXPOSURE	VFAINT
10564	2009 Oct 2	10.020	S3	TIMED EXPOSURE	VFAINT

sources. Observational details are given in Table 1. Data were reduced using the software package CIAO (ver. 3.4) with the appropriate calibration products. We created exposure maps using the task `merge_all`⁹ and we determined the positions of the point sources using the CIAO task `wavdetect`.¹⁰ A smoothed X-ray image of NGC 922 is shown in Figure 2. The X-ray point sources are marked. Counts for the point sources were extracted from regions shown in Figure 2. Background counts for each point source were extracted from an annular region around each source (these regions are not shown in

Figure 2). The counts for each source were corrected for the PSF fraction (point-spread function fraction, i.e., the fraction of counts outside the extraction region) by using a PSF with energy 1 keV. The background subtracted, PSF corrected count rate for each source at both epochs is shown in Table 2.

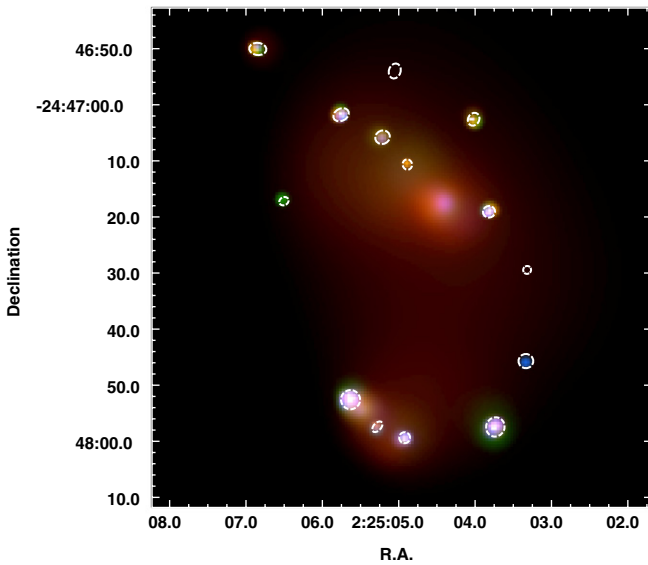
We extracted X-ray spectra and standard response files (ARF and RMF) for each source. Fluxes and luminosities for the deep March observation were constructed in the 0.3–8 keV band, assuming a galactic absorption $N_H = 1.6 \times 10^{20} \text{ cm}^{-2}$. Using the results of Swartz et al. (2004), we adopt an intrinsic source spectrum with photon index $\Gamma = 1.7$ to calculate luminosities. Fluxes were then calculated in XSPEC by rescaling the normalization of the power-law model to the observed count rates.

⁹ See http://xc.harvard.edu/ciao/threads/merge_all.

¹⁰ See http://xc.harvard.edu/ciao3.0/download/doc/detect_html_manual/Manual.html.

Table 2
NGC 922 Detected X-Ray Sources

Source	R.A.	Decl.	Net Count Rate		$F_X(0.3-8 \text{ keV})$	$L_X(0.3-8 \text{ keV})$
			March 9	Oct 9	$10^{-15} \text{ erg cm}^{-2} \text{ s}^{-1}$	$10^{39} \text{ erg s}^{-1}$
			(counts ks $^{-1}$)		March 9	March 9
1	02 25 06.84	-24 46 50.05	0.92	0.41	6.77 ± 1.25	1.86
2	02 25 06.50	-24 47 17.19	0.30	<0.1	2.49 ± 0.78	0.68
3	02 25 05.76	-24 47 01.78	1.57	2.04	14.04 ± 2.0	3.87
4	02 25 05.63	-24 47 52.58	11.47	4.78	87.80 ± 4.64	24.20
5	02 25 05.28	-24 47 57.41	0.49	1.06	4.30 ± 1.05	1.19
6	02 25 05.21	-24 47 05.79	0.44	0.80	3.74 ± 1.04	1.02
7	02 25 05.05	-24 46 53.98	0.21	<0.1	1.89 ± 0.79	0.52
8	02 25 04.92	-24 47 59.36	1.49	1.00	11.27 ± 1.65	3.10
9	02 25 04.89	-24 47 10.66	0.44	0.29	3.57 ± 0.95	0.98
10	02 25 04.02	-24 47 02.58	1.46	1.16	12.11 ± 1.77	3.33
11	02 25 03.82	-24 47 19.08	1.68	3.28	14.20 ± 1.89	3.91
12	02 25 03.74	-24 47 57.45	4.08	3.49	31.49 ± 2.81	8.67
13	02 25 03.33	-24 47 45.70	0.42	0.49	3.23 ± 0.92	0.88
14	02 25 03.32	-24 47 29.45	0.26	0.21	2.35 ± 0.77	0.64

**Figure 2.** RGB *Chandra* image of NGC 922. The three bands are—red: the 0.3–1.0 keV; green: 1.0 – 2.0 keV; and blue: 2.0 – 8.0 keV. An adaptive smoothing algorithm has been applied to the data. The extraction regions for the point sources are defined by the white ellipses.

(A color version of this figure is available in the online journal.)

Luminosities were calculated assuming a distance of 48 Mpc (Olivares et al. 2010).

3. THE X-RAY SOURCE POPULATION OF NGC 922

NGC 922 has a population of bright X-ray point sources, including nine ULXs, defined by $L_x > 10^{39} \text{ erg s}^{-1}$, in the 0.3–8.0 keV band (there are seven ULXs in the 2–10 keV band). Count rates for both the March and October observations are shown in Table 2. Many of the sources are variable. Figure 1 shows an $H\alpha$ image of NGC 922 with positions of the X-ray sources superimposed. The X-ray sources are clearly associated with recent star formation, and several are coincident with the star-forming ring. The close association of bright X-ray sources with recent star formation has been observed in many starburst galaxies (Wolter & Trinchieri 2004; Zezas et al. 2007; Rappaport et al. 2010). It is generally accepted that the X-ray

Table 3
Best-fitting Parameters for Source X-4

Parameter	Power Law	Multicolored disk
$N_{\text{H,Gal}} (\text{cm}^2)$	1.62×10^{20}	1.62×10^{20}
$N_{\text{H}} (\text{cm}^2)$	$2.4^{+1.1}_{-0.9} \times 10^{21}$	$3.4^{+3.4}_{-9.5} \times 10^{20}$
	$\gamma = 1.9^{+0.2}_{-0.3}$	$T_{\text{in}} (\text{keV}) = 1.3 \pm 0.3$
Normalization	$2.3 \pm 0.95 \times 10^{-5}$	$1.36 \pm 1.01 \times 10^{-3}$
χ^2/dof	1.15 (20.79/18)	1.15 (20.7/18)

Note. Models are `phabs*phabs*pow` and `phabs*phabs*diskbb`.source population at high luminosities ($L_x > 10^{37} \text{ erg s}^{-1}$) is dominated by accreting X-ray binaries (Fabbiano 2006).

3.1. The Brightest Source in NGC 922

NGC 922 X-4 has a 0.3–8 keV luminosity $L_x = 2 \times 10^{40} \text{ erg s}^{-1}$, placing it at the upper end of the X-ray binary luminosity function (Grimm et al. 2003; Swartz et al. 2004). The count rate declined by a factor of two in the second observation. We fit the 0.3–10 keV spectrum of NGC 922 with two models—a simple power law and a multicolored disk blackbody. In both cases, a galactic N_{H} of $1.62 \times 10^{20} \text{ cm}^{-2}$ was assumed and fixed in the fit, and another absorption component intrinsic to the source was allowed to vary. The resulting fit parameters are shown in Table 3. The luminosity, spectrum and variability of NGC 922 X-4 are typical of ULXs that appear to have hard X-ray spectra at the highest accretion rates (Gladstone et al. 2009; Berghea et al. 2008). Other examples include IC 342 X-1, NGC 1313 X-1 (Gladstone et al. 2009), NGC 1365 (Soria et al. 2009), and Holmberg IX X-1 (Kaaret & Feng 2009; Vierdayanti et al. 2010). This high flux/hard spectrum behavior is interesting because it appears to be different to what is generally observed in Galactic black hole binaries, where soft thermal emission from a disk dominates higher accretion states. The “high/hard” state as been provisionally called the “ultraluminous” state (Gladstone et al. 2009). It may correspond to a super-Eddington accretion state where an outflowing wind from the inner accretion disk leads to an increased optical depth and lower coronal temperature (Gladstone et al. 2009).

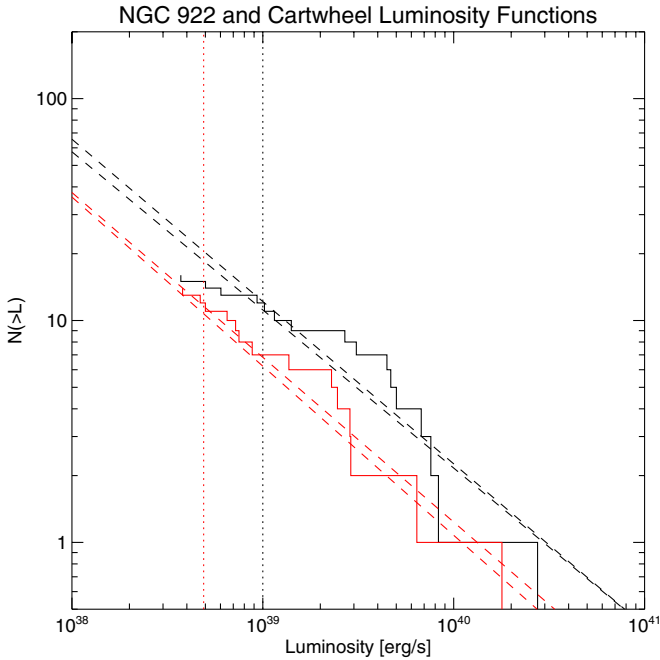


Figure 3. X-ray luminosity function of the Cartwheel galaxy (top, black) and NGC 922 (bottom, red). Two fits are shown for each galaxy: the upper fit is to the raw data, and the lower fit is corrected for background sources using the results of Giacconi et al. (2001). The vertical lines show the lower limit to the fit for the Cartwheel (black) and NGC 922 (red).

(A color version of this figure is available in the online journal.)

3.2. Comparison with the Cartwheel

Here we compare the ULX population seen in NGC 922 with that of the Cartwheel. The Cartwheel has a metallicity in the range $Z \sim 0.18\text{--}0.3 Z_{\odot}$ in the ring (Fosbury & Hawarden 1977; Vorobyov & Bizyaev 2001). This is considerably lower than the metallicity of NGC 922, which is $\sim 0.75 Z_{\odot}$ (Wong et al. 2006). Figure 3 shows the cumulative luminosity function for sources in NGC 922 and the Cartwheel. Luminosities for sources in the Cartwheel were taken from Wolter & Trinchieri (2004). In order to check that there were no systematic differences in fluxes derived using our method (described in Section 2) and that used by Wolter & Trinchieri (2004) we repeated our analysis using the archival Cartwheel data. We derived fluxes essentially identical to Wolter & Trinchieri (2004). We note that luminosities for X-ray sources in the Cartwheel are calculated in the 2–10 keV band (Wolter & Trinchieri 2004). The X-ray luminosities of sources in NGC 922 have been plotted in the 2–10 keV band in order to allow for direct comparison with the Cartwheel. This results in slightly lower luminosities than given in Table 2. There are seven ULXs in NGC 922 in the 2–10 keV band.

We fit a single power law to the unbinned, differential, XLFs using a maximum likelihood statistic (Crawford et al. 1970). The goodness-of-fit (GOF) estimate is performed by simulating a luminosity distribution with the best-fit slope. One million iterations were performed. If the data are well fitted by a single power law, the GOF statistic approaches 1.0. The contribution of cosmic background sources to the XLF was evaluated using the log N –log S curves of Giacconi et al. (2001). Details of the fitting method are given in Kilgard et al. (2005). Table 4 gives the results.

Table 4 shows that the XLF slopes of high-luminosity X-ray sources in the Cartwheel and NGC 922 are identical within the uncertainties. The slopes are consistent with the “Universal”

Table 4
Power-law Fits to the XLF

Galaxy	γ	L_{\min} (erg s^{-1})	GOF	N_{fit}	N_{39}
Cartwheel	0.71 ± 0.120	1×10^{39}	0.81	12.0	11.1
NGC 922	0.76 ± 0.22	5×10^{38}	0.71	14	7.5

Notes. γ is the fitted slope to the XLF correcting for background sources. L_{\min} is the minimum luminosity included in the fit. GOF is the goodness-of-fit parameter. N_{fit} is the number of sources included in the fit, and N_{39} is the predicted number of ULXs (i.e., sources with $L_x > 10^{39} \text{ erg s}^{-1}$).

high-mass X-ray binary XLF described by Grimm et al. (2003). Assuming that the star formation rates of the Cartwheel and NGC 922 are 18 and $8 M_{\odot} \text{ yr}^{-1}$ respectively (Mayya et al. 2005; Wong et al. 2006), we find that the number of ULX sources relative to the star formation rate is 0.94 ± 0.3 ULX per solar mass of star formation for NGC 922, and 0.67 ± 0.2 ULX per solar mass of star formation for the Cartwheel. Here we use the number of ULX in the 2–10 keV band. These ratios are dependant on the assumed star formation rates. The star formation rates quoted for NGC 922 and the Cartwheel were derived using extinction-corrected $H\alpha$ luminosities. There is no evidence for widespread obscured star formation in either galaxy, so these values are likely to be close to the correct values. We conclude that there is no evidence for an excess of high-luminosity sources (normalized to the star formation rate) in the lower-metallicity Cartwheel unless the SFR of either galaxy is wrong by a factor of two or more.

4. POPULATION SYNTHESIS MODELS

The similar ULX/SFR observed in the Cartwheel and NGC 922 is, in fact, expected in population synthesis models of ULX formation in low-metallicity environments. Linden et al. (2010) studied the mechanisms for high-mass X-ray binary formation in starburst environments, finding the ULX population to be dominated by systems moving through pathways powered by strong wind accretion from supergiant donors onto massive black holes formed in failed supernovae at both $Z = 0.75 Z_{\odot}$ and $Z = 0.28 Z_{\odot}$.

Utilizing simulations from the StarTrack code (Belczynski et al. 2008) simulations using an SFR of $18 M_{\odot} \text{ yr}^{-1}$ for the Cartwheel and $8 M_{\odot} \text{ yr}^{-1}$ for NGC 922¹¹ we calculate a population of 103 ULXs for NGC 922 and 238 ULXs for the Cartwheel. We note two results: (1) our default simulations overpredict the absolute number of observed systems by approximately an order of magnitude, and (2) our models similarly predict no metallicity dependence in the ULX/SFR ratio in the regime between $0.75 Z_{\odot}$ and $0.3 Z_{\odot}$ investigated in this study.

Predictions regarding the absolute number of bright X-ray binaries are particularly difficult for population synthesis models. We note several obvious parameter space choices which would allow a match between our simulations and observations. Because the supergiant donors have extremely large radii, the ULX formed through this pathway must be weakly bound—implying that small natal kicks imparted to massive black holes (BHs; e.g., a Maxwellian distribution with dispersion velocity 26.5 km s^{-1}) can disrupt as many as 90%

¹¹ The continuous star formation period is simulated to last for 100 Myr. However, a negligible number of ULXs are produced after 20 Myr, rendering the exact end of the simulation unimportant.

of ULX progenitors (Linden et al. 2010). Additionally, our definition of ULX assumes an average X-ray luminosity of 1×10^{39} erg s⁻¹, however eccentricities may make these systems dimmer for a substantial portion of their orbit. Another plausible explanation concerns the treatment of super-Eddington accretion. In our default simulations we allow black hole accretors to power ULXs at up to ten times the Eddington limit, so long as the donor winds are able to supply enough material to the black hole accretor. Our models do not describe the specific mechanisms which allow this. Several mechanisms involving dynamic instabilities have been postulated and include leaky-disk (Begelman 2002) or beaming (King et al. 2001) models which may imply a duty cycle at the 10% level.

The ratio of ULX formation rates between NGC 922 and the Cartwheel places more meaningful constraints on the models than absolute numbers, as there are fewer parameters which can fine tune the metallicity dependence. In this case, we find models using the default assumptions in Linden et al. (2010) to correctly predict insignificant metallicity dependence in the regime from $Z = 0.75 Z_{\odot}$ to $Z = 0.18 Z_{\odot}$. We emphasize that this relation falls naturally out of our simulations, as the ULX population at both metallicities is created through the same evolutionary channels. We note that if the metallicity of the Cartwheel is significantly lower than assumed here, then this assumption would no longer hold, and the Cartwheel would begin to be dominated by a second population powered by Roche Lobe overflow of main-sequence stars onto fallback BH accretors (this model has been suggested as a mechanism to explain the properties of the brightest source in the Cartwheel; Pizzolato et al. 2010). Thus, the consistency of the ULX/SFR ratio provides some preference for a higher modeled metallicity within the Cartwheel. Guided by this consistency in the ULX/SFR in the observed metallicity range, we note several other robust results. First, the supergiant donors which power ULX activity die off quickly after star formation, and we find $\sim 95\%$ of luminous ULXs to be younger than 20 Myr. Second, the direct collapse pathway imparts almost no systematic velocity to the resultant X-ray binaries, and thus ULXs are constrained to lie very close to recent star formation regions. However, these systems may gain significant spatial velocities if they are formed within dense stellar environments where three body interactions become non-negligible (Mapelli et al. 2011). Finally, we caution that the significant overabundance of ULX sources predicted by StarTrack models implies an additional physical mechanism which must eliminate a large number of possible ULX systems. We are unable, in this study, to constrain this mechanism from introducing a metallicity dependence, which would create a mismatch between observations and our simulated population.

5. SUMMARY AND CONCLUSIONS

NGC 922 is a drop-through ring galaxy (Wong et al. 2006) with an expanding ring of star formation, similar in many respects to the Cartwheel galaxy. New *Chandra* observations reveal a population of bright X-ray point sources, including nine ULXs, defined by $L_x > 10^{39}$ erg s⁻¹ in the 0.3–8.0 keV band. The brightest source has a 0.3–8 keV luminosity $L_x = 2 \times 10^{40}$ erg s⁻¹, placing it at the upper end of the X-ray binary luminosity function (Grimm et al. 2003; Swartz et al. 2004). The spectrum of this source is hard and similar to other binaries in an “ultraluminous” state (Gladstone et al. 2009; Berghea et al. 2008).

We compare the NGC 922 X-ray source population with that of the Cartwheel. These two systems are similar in many respects (both drop-through ring galaxies) but the Cartwheel has a lower metallicity than NGC 922. We find that the number of ULXs in NGC 922 and the Cartwheel scales with the star formation rate: there is no evidence for an excess of sources in the Cartwheel.

Population synthesis models using *StarTrack* suggest that the ULX population in both NGC 922 and the Cartwheel is dominated by systems with strong wind accretion from supergiant donors onto direct-collapse BHs. The default models overpredict the number of observed ULXs in both galaxies. There are several simplifying assumptions in the simulations which could account for the discrepancy. For example, the models assume that direct collapse events impart no natal kick to the resultant black hole. However, even small kicks could separate the widely spaced progenitors before the ULX phase begins, hence reducing the number of ULXs. The simulations correctly predict the ratio of the number of ULXs in NGC 922 and the Cartwheel. We emphasize that this relation falls naturally out of the Linden et al. (2010) simulations, as the ULX population at both metallicities is created through the same evolutionary channels. We note that the Linden et al. (2010) simulations predict a substantially different ULX population below $Z < 0.15 Z_{\odot}$. Thus, it would appear that the metallicity of the Cartwheel is not low enough to see a difference in the ULX population compared to NGC 922. We are currently working on a project to search for ULXs in Extremely Metal Poor Galaxies. These are the most metal-poor galaxies known, and a logical place to find ULXs if they favor metal-poor systems. We will report on these findings in a future paper.

We thank the referee for comments which improved this paper. Support for this work was provided by the National Aeronautics and Space Administration through Chandra Award Number GO9-0097A issued by the Chandra X-ray Observatory Center, which is operated by the Smithsonian Astrophysical Observatory for and on behalf of the National Aeronautics Space Administration under contract NAS8-03060. This research has made use of the NASA/IPAC Extragalactic Database (NED) which is operated by the Jet Propulsion Laboratory, California Institute of Technology, under contract with the National Aeronautics and Space Administration. G.T. and A.W. acknowledge partial financial contribution from the ASI-INAF agreement I/009/10/0.

REFERENCES

- Begelman, M. C. 2002, *ApJ*, 568, L97
 Belczynski, K., Kalogera, V., Rasio, F. A., et al. 2008, *ApJS*, 174, 223
 Belczynski, K., Sadowski, A., & Rasio, F. A. 2004, *ApJ*, 611, 1068
 Berghea, C. T., Weaver, K. A., Colbert, E. J. M., & Roberts, T. P. 2008, *ApJ*, 687, 471
 Block, D. L., Puerari, I., Takamiya, M., et al. 2001, *A&A*, 371, 393
 Crawford, D. F., Jauncey, D. L., & Murdoch, H. S. 1970, *ApJ*, 162, 405
 Fabbiano, G. 2006, *ARA&A*, 44, 323
 Fosbury, R. A. E., & Hawarden, T. G. 1977, *MNRAS*, 178, 473
 Gao, Y., Wang, Q. D., Appleton, P. N., & Lucas, R. A. 2003, *ApJ*, 596, L171
 Giacconi, R., Rosati, P., Tozzi, P., et al. 2001, *ApJ*, 551, 624
 Gladstone, J. C., Roberts, T. P., & Done, C. 2009, *MNRAS*, 397, 1836
 Grimm, H.-J., Gilfanov, M., & Sunyaev, R. 2003, *MNRAS*, 339, 793
 Kaaret, P., & Feng, H. 2009, *ApJ*, 702, 1679
 Kilgard, R. E., Cowan, J. J., Garcia, M. R., et al. 2005, *ApJS*, 159, 214
 King, A. R., Davies, M. B., Ward, M. J., Fabbiano, G., & Elvis, M. 2001, *ApJ*, 552, L109
 Linden, T., Kalogera, V., Sepinsky, J. F., et al. 2010, *ApJ*, 725, 1984
 Mapelli, M., Colpi, M., & Zampieri, L. 2009, *MNRAS*, 395, L71

- Mapelli, M., Ripamonti, E., Zampieri, L., & Colpi, M. 2011, *MNRAS*, **416**, 1756
- Mayya, Y. D., Bizyaev, D., Romano, R., Garcia-Barreto, J. A., & Vorobyov, E. I. 2005, *ApJ*, **620**, L35
- Meurer, G. R., Hanish, D. J., Ferguson, H. C., et al. 2006, *ApJS*, **165**, 307
- Olivares, E. F., Hamuy, M., Pignata, G., et al. 2010, *ApJ*, **715**, 833
- Pellerin, A., Meurer, G. R., Bekki, K., et al. 2010, *AJ*, **139**, 1369
- Pizzolato, F., Wolter, A., & Trinchieri, G. 2010, *MNRAS*, **406**, 1116
- Rappaport, S., Levine, A., Pooley, D., & Steinhorn, B. 2010, *ApJ*, **721**, 1348
- Roberts, T. P. 2007, *Ap&SS*, **311**, 203
- Soria, R., Cropper, M., Pakull, M., Mushotzky, R., & Wu, K. 2005, *MNRAS*, **356**, 12
- Soria, R., Risaliti, G., Elvis, M., et al. 2009, *ApJ*, **695**, 1614
- Swartz, D. A., Ghosh, K. K., Tennant, A. F., & Wu, K. 2004, *ApJS*, **154**, 519
- Vierdayanti, K., Done, C., Roberts, T. P., & Mineshige, S. 2010, *MNRAS*, **403**, 1206
- Vorobyov, E. I., & Bizyaev, D. 2001, *A&A*, **377**, 835
- Wolter, A., & Trinchieri, G. 2004, *A&A*, **426**, 787
- Wong, O. I., Meurer, G. R., Bekki, K., et al. 2006, *MNRAS*, **370**, 1607
- Zezas, A., Fabbiano, G., Baldi, A., et al. 2007, *ApJ*, **661**, 135
- Zezas, A., Fabbiano, G., Rots, A. H., & Murray, S. S. 2002, *ApJ*, **577**, 710